

N-Body Simulations with REBOUND

Lab Course Protocol

Group 3

Sin-iu Ho

March 6, 2023

Advanced lab course in astronomy
Eberhard Karls Universität Tübingen

WiSe 2022/23

Abstract

Contents

1	The two-body problem	1
2	The co-planar three-body Problem	5
2.1	Theory	5
2.2	Setup	6
2.3	Result	7
3	Stability of Saturn's rings	11
3.1	Theory	11
3.2	Setup	11
3.3	Result	12
4	Jupiter and Kirkwood gaps	14
5	Resonant capture of planet	16
5.1	Trial 1	17
5.2	Trial 2	17

1 The two-body problem

In this exercise, we study a two-body system with the the following setup:

Table 1: Setup of Section 1.

Object	m	a	e
Primary	1.0		
Planet	1.0×10^{-3}	0.1	0.3

We are especially concerned with the numerical accuracy of different [integrators](#). So we run the simulation of the system for 1000 cycles/orbits (`Norbits = 1000`), each of which is completed by one step (`stepperorbit = 1`). Meanwhile, we use an iterator to repeat the simulation with four (or six) different time steps (`sim.dt = Δt = 10-1, 10-2, …, 10-6`). Every time when the integrator “steps forward”, several parameters of the planet are recorded, including the coordinates (x, y) , energy E , angular momentum L_z , semi-major axis a , eccentricity e , and argument of pericenter ω .

According to theory, those quantities are conserved, which means that any deviation from their initial value can be attributed to numerical error.

Fig. 1 shows the results of `leapfrog` integrator; while Fig. 2 shows the result of `IAS15` integrators. Since the errors are extremely tiny, logarithmic scale. Next, one can observe:

- `leapfrog`’s results have more distinguishable periodical patterns;
- generally speaking, `leapfrog`’s errors are larger than those of `IAS15`;
- `leapfrog`’s results have more distinguishable periodical patterns; 2) generally speaking.

To obtain a better correlation between time steps and errors, one might plot the errors of parameters over time steps as in Fig. 3. Surprisingly, for `leapfrog`, only the error of angular momentum decreases with time step $Δt$; the other parameters seem to increase with time in power law (we haven’t done the regression, though). On the other hand, for `IAS15`, there is only a slight change in error when we apply finer time steps.

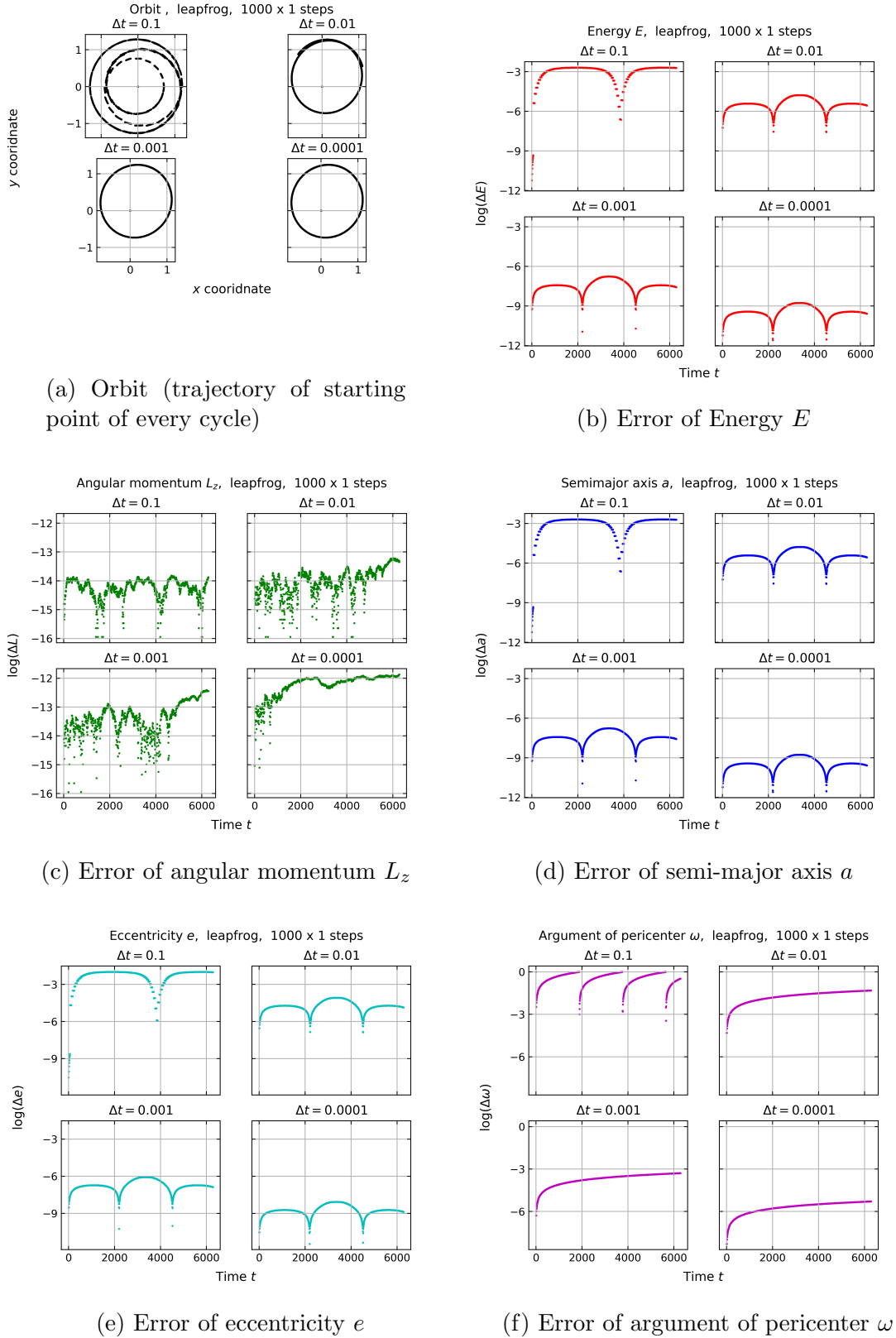


Figure 1: Errors of parameters (in logarithmic scale) with 4 different fixed time-steps (4 panels in each subfigure); leapfrog integrator

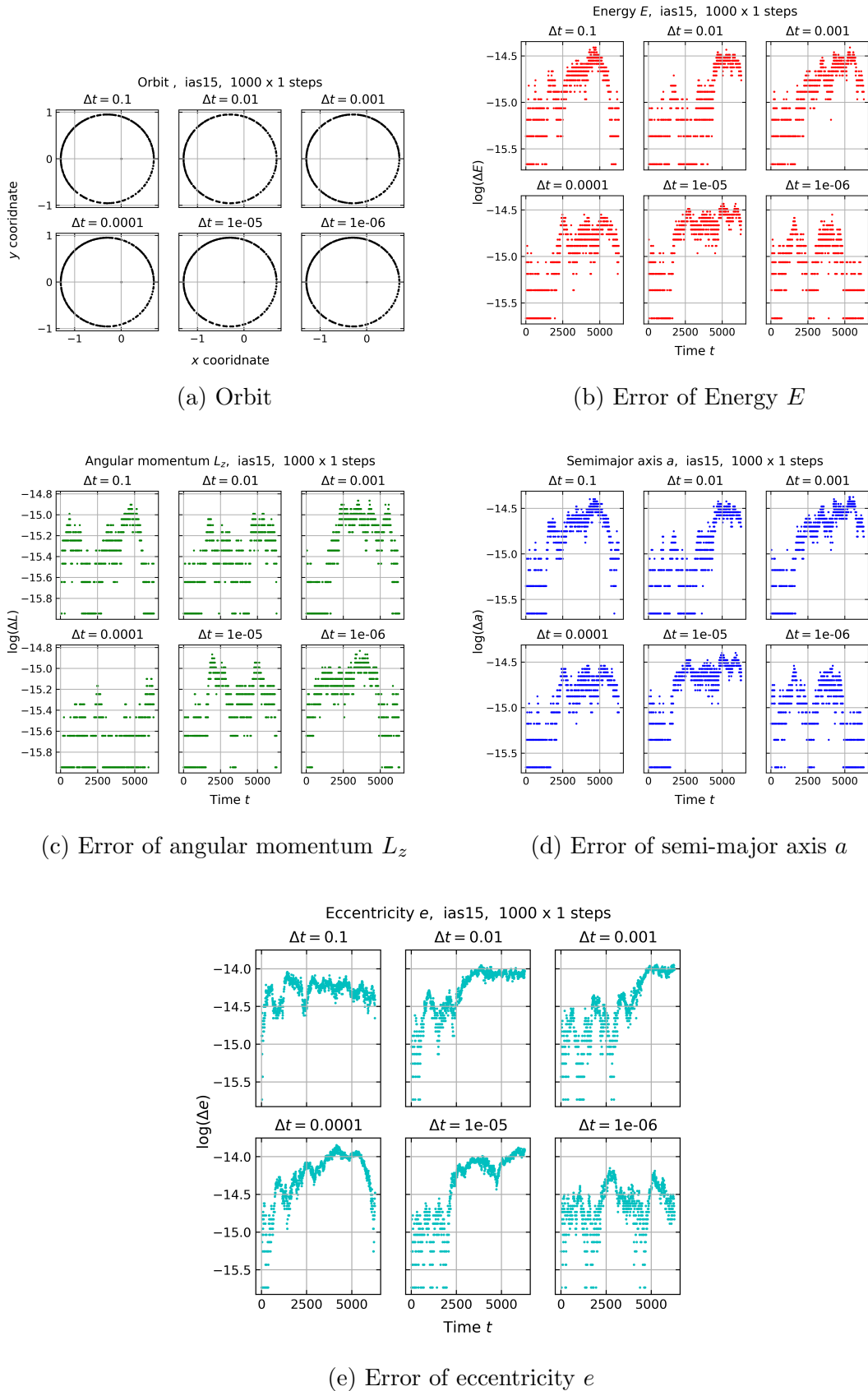
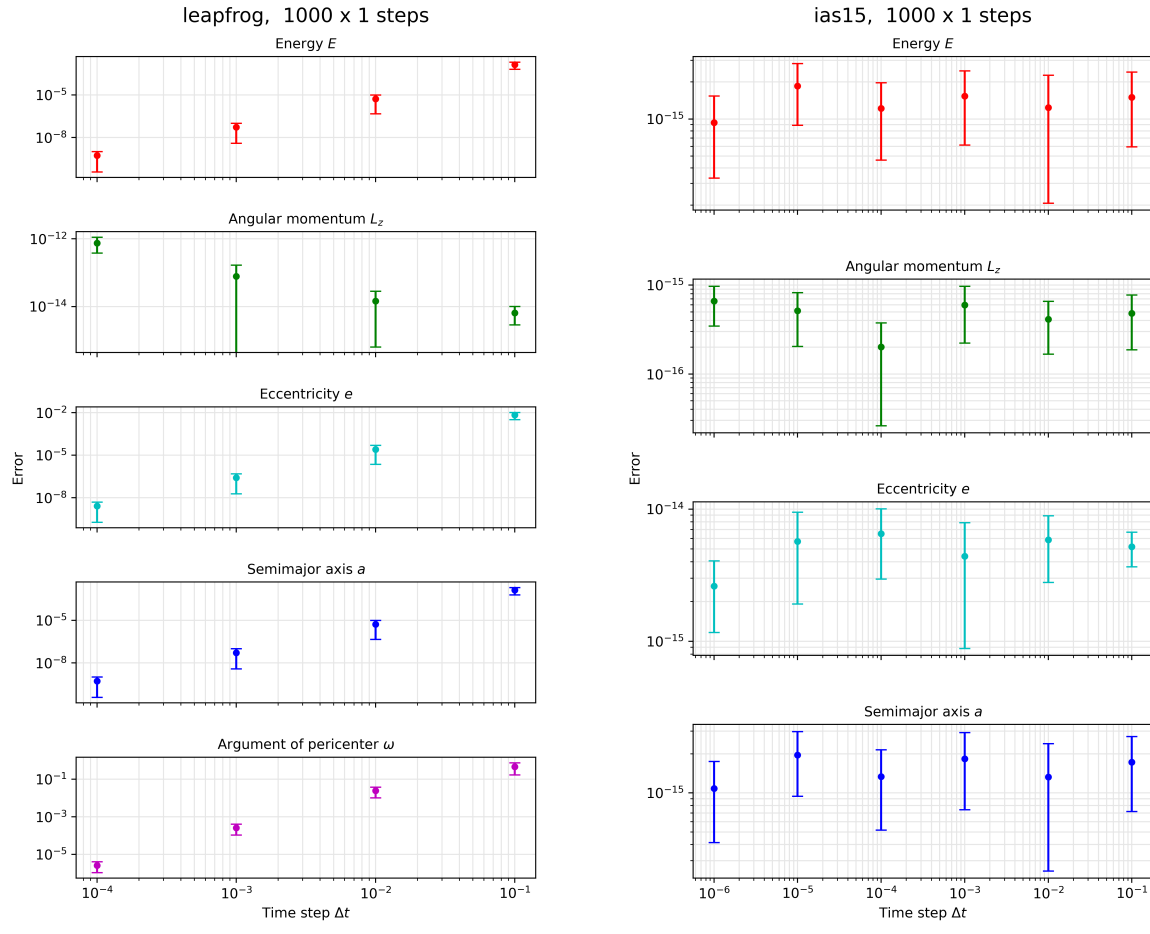


Figure 2: Errors of parameters (in logarithmic scale) with different fixed time-steps (6 panels in each subfigure); IAS15 integrator



(a) Error of leapfrog integrator

(b) Error of IAS15 integrator

Figure 3: Error comparison (logarithmic scale) between leapfrog and IAS15 integrator. The data points are the average over the entire duration; and the error bars are the standard deviations.

2 The co-planar three-body Problem

2.1 Theory

Consider a three-body problem with configuration shown in Fig. 4, where two planets with masses m_1 and m_2 are orbiting a much more massive star with mass M on the same plane. Even though the two planets are placed in opposition initially, the separation Δ in orbits will lead to different orbital periods and thus the conjunctions from time to time, at which the two planets are likely to be close enough to affect each other's orbits through perturbations. The smaller Δ is, the more perturbations can be expected, and the more unstable the system will be.

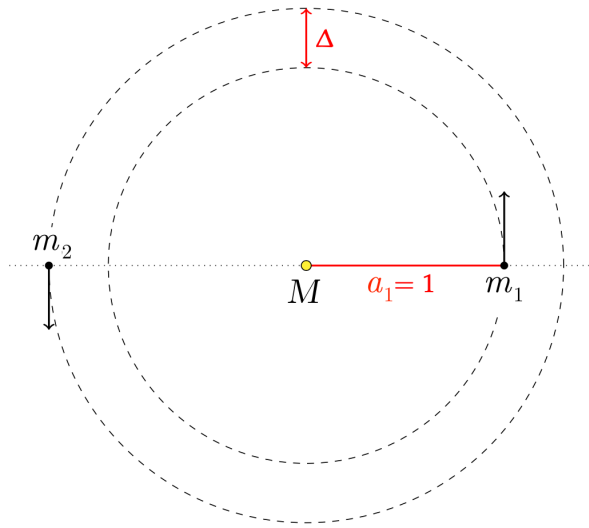


Figure 4: Configuration of Section 2.

Gladman[1] shows that, for a co-planar three-body Problem prescribed above, the criterion for the system to be stable against any close encounter is

$$\Delta > \Delta_c \simeq 2.4 \left(\frac{m_1}{M} + \frac{m_2}{M} \right)^{1/3}. \quad (1)$$

Here, a close encounter is defined as an occurrence when the distance of two planets is less than the Hill radius of the star:

$$R_{\text{Hill}} \approx a \sqrt[3]{\frac{m}{3M}}, \quad (2)$$

where a is the semi-major axis; m and M are the masses of the planet and the star, respectively.

2.2 Setup

In this exercise, we seek to examine the validity of critical separation Δ_c given by Eq. (1). We use the `ias15` integrator to execute the simulation for 10000 orbital periods¹ with 100 steps per orbit. The two setups that we use are given in Table 2. For each setup, five ratios of initial separation Δ/Δ_c will be iterated over the program: 10 %, 50 %, 100 %, 150 %, 1000 %. Besides, the data of semi-major axes a and eccentricities e of both planets is recorded so that the time evolution $a(t)$ and $e(t)$ can be plotted. If there is at least one close encounter found in the 10000 orbital periods, then the system is considered unstable; otherwise, it is considered stable.

Table 2: Setup 1 (or Setup 2) for Section 2

Object	Mass	Hill radius	Semi-major axis	Eccentricity	Argument of periastron
	m/M_\odot	$R_{\text{Hill}}/\text{AU}$	a/AU	e	ω/rad
Star	1.0				
Planet 1	1.0×10^{-5}	0.0149	1.0	0.0	0
Planet 2	1.0×10^{-5a}	0.0049	$1.0 + \Delta^b$	0.0	π

^a Setup 2 differs from Setup 1 only in that $m_2 = 1.0 \times 10^{-7} M_\odot$.

^b Different values of orbital separation Δ will iterate in our program.

Importantly, the close encounters are detected by the `direct` collision module. It uses the method `sim.collision_resolve` to call our customized function `collision_print_only` whenever it finds an overlap between Hill spheres during the integration so that we can count (or optionally print the time) and analyze the number of close contacts. Fig. 5 is a specific example of close encounter. One can see both planets are subject to a drastic change in semi-major axis due to perturbation; in the meantime, the distance between planets breaks the lower limit, which is the sum of Hill radii.

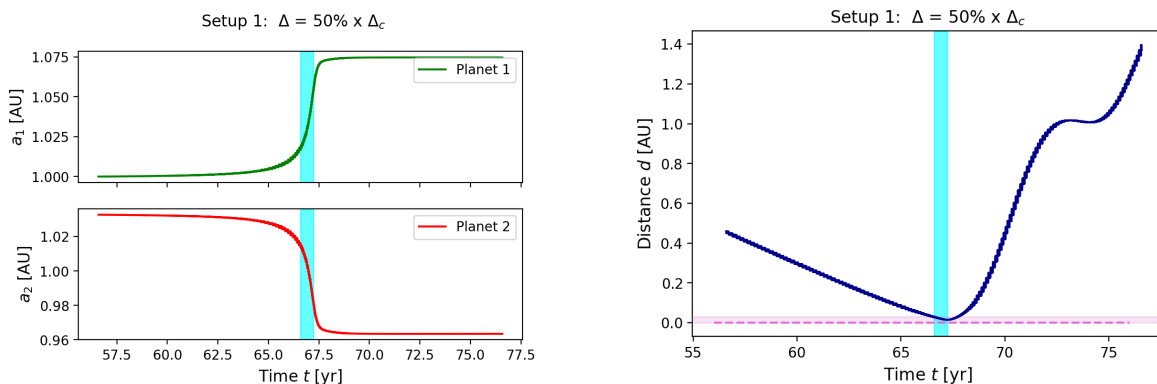


Figure 5: Close-ups of time evolution of the semi-major axes of both planets (left) and the distance between them (right). The cyan vertical spans represent the close encounter at $t \approx 67.0$ yr. The horizontal span at the bottom of the right subfigure is the range within the sum of Hill radii ($d \lesssim 0.02$ AU).

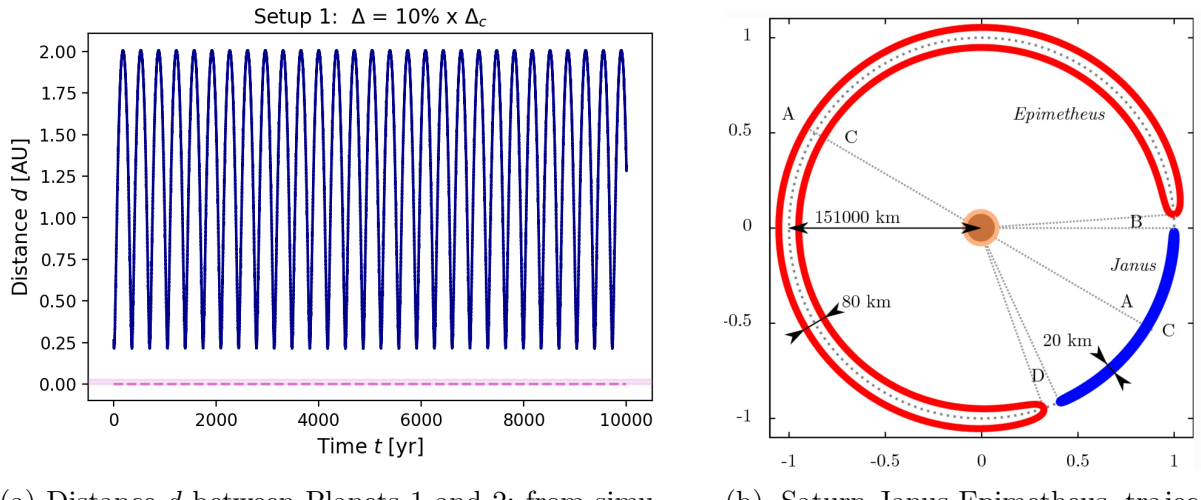
¹Base on our setups, every orbital period lasts about 2π time units in REBOUND, or equivalently 1 year.

2.3 Result

The result is summarized in Table 3. The related plots of time evolution $a(t)$ and $e(t)$ for Setup 1 is shown in Fig. 7, and for Setup 2, in Fig. 8.

Looking at these simulation results, some key points can be drawn. First of all, since all the cases with $\Delta > \Delta_c$ are found to be stable and the unstable cases only occurs when $\Delta \leq \Delta_c$, the criterion of Eq. (1) is supported by numerical evidence. If time permits, one can also try more different values of Δ with finer intervals to determine the numerical criterion of stability.

Secondly, it is worth noting that the cases with $\Delta = 10\% \times \Delta_c$ still produce stable systems even if their initial orbital separation are not in the range given by Eq. (1). The top subfigures in Fig. 7 show that there have been no significant changes on the circular orbits with initial radius. Also, from an extra plot shown in Fig. 6a one sees that the distance between the two planets oscillates periodically, but never falls below ~ 0.22 AU. A possible explanation for this behavior is that the planets have a pair of horseshoe orbits like those in Saturn-Janus-Epimetheus system (Fig. 6b). To prove this conjecture, one must also draw the evolution of mean longitude against time.



(a) Distance d between Planets 1 and 2; from simulation of Setup 1

(b) Saturn-Janus-Epimetheus trajectories; excerpted from [3].

Figure 6: Possible explanation for the orbits with $\Delta = 10\% \times \Delta_c$.

Next, from the stable cases seen in Figs. 7 and 8, one can observe the periodic patterns of perturbation. Careful observation reveals that the period shows negative correlation with the orbital separation Δ . (Note that the bottom two or three rows of subfigures in Figs. 7 and 8 have been zoomed in along the time axis.) This can be explained by the following consideration. Given that the features on periodic patterns are caused by perturbation, which takes place when two planets are in a conjunction, we can calculate the synodic period T_{syn} (i.e., the time between two consecutive conjunctions) of two planets, which is

$$T_{\text{syn}} = \left(\frac{1}{T_1} - \frac{1}{T_2} \right)^{-1} = \frac{T_1}{1 - T_1/T_2}, \quad (3)$$

where T_1 and T_2 denote the periods of Planet 1 and Planet 2, respectively. But Kepler's third law states $T^2 = (4\pi^2/GM)a^3$; hence, in our configuration, where a_1 is fixed to 1 AU

and T_1 is fixed to 1 yr, T_{syn} can be described by

$$T_{\text{syn}} = \frac{T_1}{1 - (a_1/a_2)^{3/2}} = \frac{1 \text{ yr}}{1 - (1 + \Delta/\text{AU})^{-3/2}}. \quad (4)$$

Therefore, the closer the orbits, the more frequent perturbation is expected. One can do a Fourier analysis of the time evolution to gain more insight into the perturbation patterns.

Last but not least, the fluctuations of $a(t)$ and $e(t)$ for the stable cases are dependent on the mass ratio m_1/m_2 and the orbital separation Δ of two planets. Roughly speaking, the fluctuations of $a(t)$ and $e(t)$ are inversely proportional to both m_1/m_2 and Δ . But this is simply a hypothesis and needs further theoretical and numerical verification.

Table 3: Results of Section 2

Orbital separation		Setup 1		Setup 2	
Δ/Δ_c	Δ/AU	Encounter	Stability	Encounter	Stability
10 %	0.0065	0	stable	0	stable
50 %	0.0326	43	unstable	24	unstable
100 %	0.0651	0	stable	3	unstable
150 %	0.0977	0	stable	0	stable
1000 %	0.6515	0	stable	0	stable

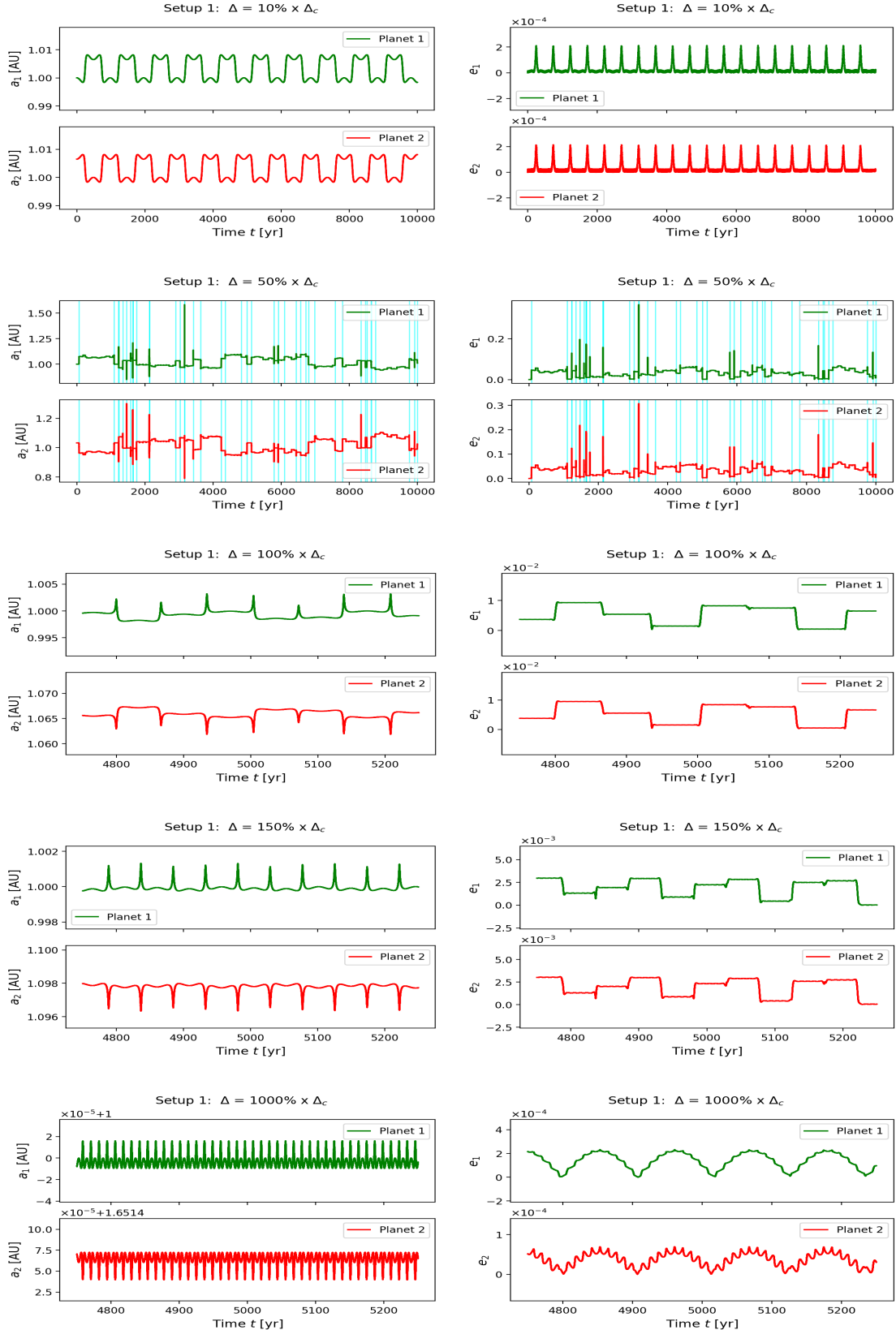


Figure 7: Time evolution of semi-major axis $a(t)$ (left column) and eccentricity $e(t)$ (right column); using Setup 1. The subfigures of each row represent different values for Δ . The cyan vertical lines represent close encounters. To make the periodicity clearly visible, the subfigures in the bottom 3 rows are zoomed in along the time axis.

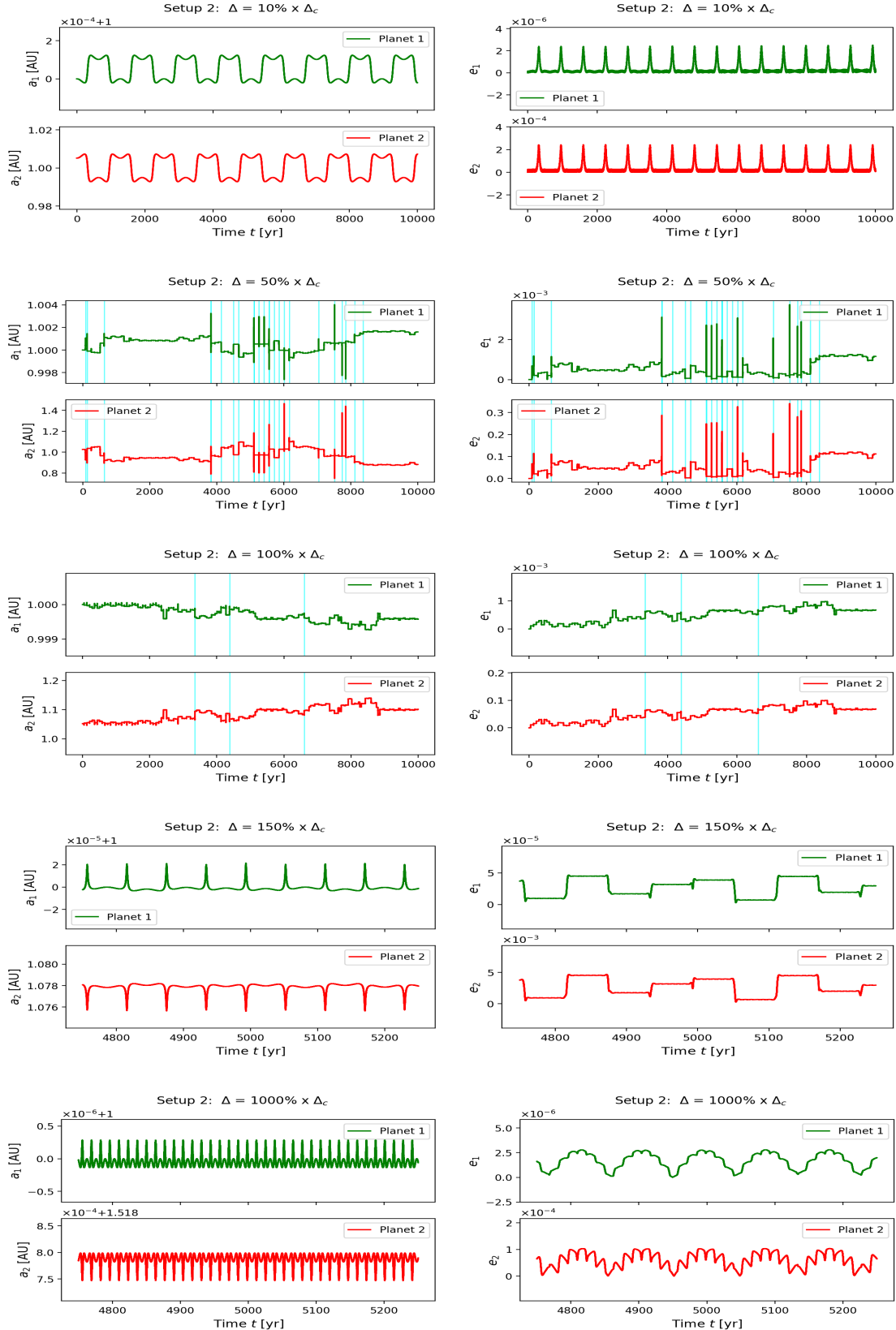


Figure 8: Time evolution of semi-major axis $a(t)$ (left column) and eccentricity $e(t)$ (right column); using Setup 2. The subfigures of each row represent different values for Δ . The cyan vertical lines represent close encounters. To make the periodicity clearly visible, the subfigures in the bottom 2 rows are zoomed in along the time axis.

3 Stability of Saturn's rings

3.1 Theory

Consider the following configuration that resembles the system of Saturn and its ring(s): n equal-mass small objects with mass m are orbiting a primary object with mass M in a circular orbit with radius r .

Vanderbei & Kolemen give a self-contained modern linear stability analysis on this problem in [2] and they conclude that the system is linear stable as long as

$$m \leq m_c = \frac{\gamma^2 M}{n^3} \quad (5)$$

with the values for γ given in

Table 4: Values for the parameter γ .

n	γ		
	theoretical[2]	numerical[2]	numerical, our work
8	2.412	2.4121	2.442 ± 0.006
10	2.375	2.3753	2.393 ± 0.006
36	2.306	2.3066	2.323 ± 0.006
100	2.300	2.2299	2.317 ± 0.006

3.2 Setup

The goal of this exercise is to reproduce the result in the third column of Table 4. We use the `leapfrog` integrator with timestep 10^5 times orbital periods and integrate for 100 orbital periods.

The radius of the small bodies (the ring) is set to be $r = 1.0$ AU. The mass of the primary object is set to be $M = 2.85716656 \times 10^{-4} M_{\odot}$ (Saturn's mass). We substitutes the theoretical values of γ in Table 4 into Eq. (5) to estimate theoretical values of m_c , and then we let the mass of small body iterate over an arithmetic sequence $\{0.90 m_c, 0.91 m_c, 0.92 m_c, \dots, 1.09 m_c\}$. The stability of the system is then diagnosed and one of the mass values will turn out to be the critical value that separates stable and unstable systems.

The initialization of the small bodies can be done with the Cartesian coordinates of position and velocities, all of which can be derived from the same initial angular velocity ω_0 . When calculating this angular velocity, the mass of small bodies should also be taken into account. The resulting formula for the initial angular velocity is

$$\omega = \sqrt{\frac{GM}{r^3} + \frac{GmI_n}{r^3}}, \quad (6)$$

where

$$I_n = \sum_{k=1}^{n-1} \frac{1}{4} \frac{1}{\sin(\pi k/n)}. \quad (7)$$

Thus, the initial tangential velocity is $v = r\omega$, and the position and the velocity of the i -th small body are ($i = 0, 1, \dots, n - 1$)

$$\begin{aligned} x_i &= r \cos(2\pi i/n), \\ y_i &= r \sin(2\pi i/n), \\ v_{x,i} &= -v \sin(2\pi i/n), \\ v_{y,i} &= v \cos(2\pi i/n). \end{aligned}$$

According to [4], the definition of stability for the system is that “the masses are still orbiting Saturn (at the end of the simulation),” which leaves some extent of vagueness. If we only view the circular and elliptic trajectories as “orbit” and exclude the parabolic or hyperbolic ones, then one of the appropriate methods of diagnosing stability is to examine at the end of simulation if there is any object with eccentricity $e \geq 1$. Of course this method not the only option. Another method is to detect negative periods P , which are also attributed to parabolic or hyperbolic orbits.

3.3 Result

Fig. 9 shows examples of the stable and the unstable case. It is evident to see that the system behaves very differently between the case with mass right above m_c and right below m_c . In the stable systems, the small bodies orbit the primary equal-distantly just as they do in the beginning; while in the unstable systems, one or more small bodies are catapulted into the distance by their mutual gravitational attraction.²

The result of our program is listed in Table 5. It is found that the critical mass value for stability is $1.02m_c$ or $1.03m_c$. From the relation $m_c \propto \gamma^2$ in Eq. (5), we can find the numerical values of γ , as listed in the rightmost column of Table 4. Our values are 1% larger than the theoretical values of [2]. The precision should be improved if finer interval of mass values are used.

²In this case, one may consider remove the small objects that are too far away from the primary object, because they will be isolated from the effects of gravity and removing them can reduce the burden of calculation.

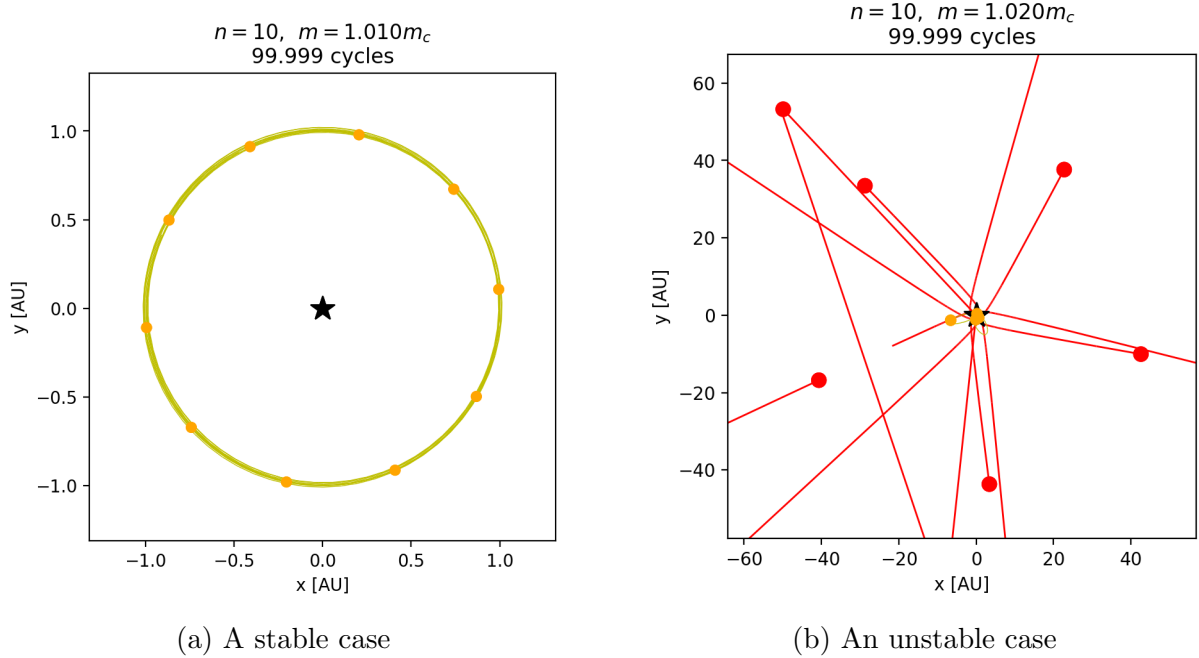
Figure 9: Two completely different simulation results; $n = 10$.

Table 5: Stability of systems with different object numbers n and masses m . The numbers in the parentheses refer to the number of small bodies which are no longer orbiting.

m/m_c	$n = 8$	$n = 10$	$n = 36$	$n = 100$
0.900	stable	stable	stable	stable
0.910	stable	stable	stable	stable
0.920	stable	stable	stable	stable
0.930	stable	stable	stable	stable
0.940	stable	stable	stable	stable
0.950	stable	stable	stable	stable
0.960	stable	stable	stable	stable
0.970	stable	stable	stable	stable
0.980	stable	stable	stable	stable
0.990	stable	stable	stable	stable
1.000	stable	stable	stable	stable
1.010	stable	stable	stable	stable
1.020	stable	unstable (6)	unstable (6)	unstable (13)
1.030	unstable (4)	unstable (10)	unstable (11)	unstable (8)
1.040	unstable (3)	stable	unstable (5)	unstable (11)
1.050	unstable (3)	unstable (6)	unstable (11)	unstable (9)
1.060	unstable (2)	unstable (10)	unstable (12)	unstable (13)
1.070	unstable (4)	unstable (8)	unstable (14)	unstable (15)
1.080	unstable (6)	unstable (5)	unstable (7)	unstable (19)
1.090	unstable (7)	unstable (3)	unstable (8)	unstable (13)

4 Jupiter and Kirkwood gaps

In this exercise, we initialize not only Mars and Jupiter with their real orbital parameters, but also 10000 (inactive) asteroids with random arguments of perihelion, random true anomalies, random eccentricities and semi-major axes ranging between 2 AU and 4 AU.

We run the simulation for 100 000 years, make two plots every 20 000 years, and observe the evolution of system. One plot is a scatter plot of eccentricity over semi-major axis, and the other is a histogram of the semi-major axes of asteroids (Figs. 10 and 11). To examine the existence of Kirkwood gaps, we also plot a zoomed-in version at the end of simulation. Fig. 12

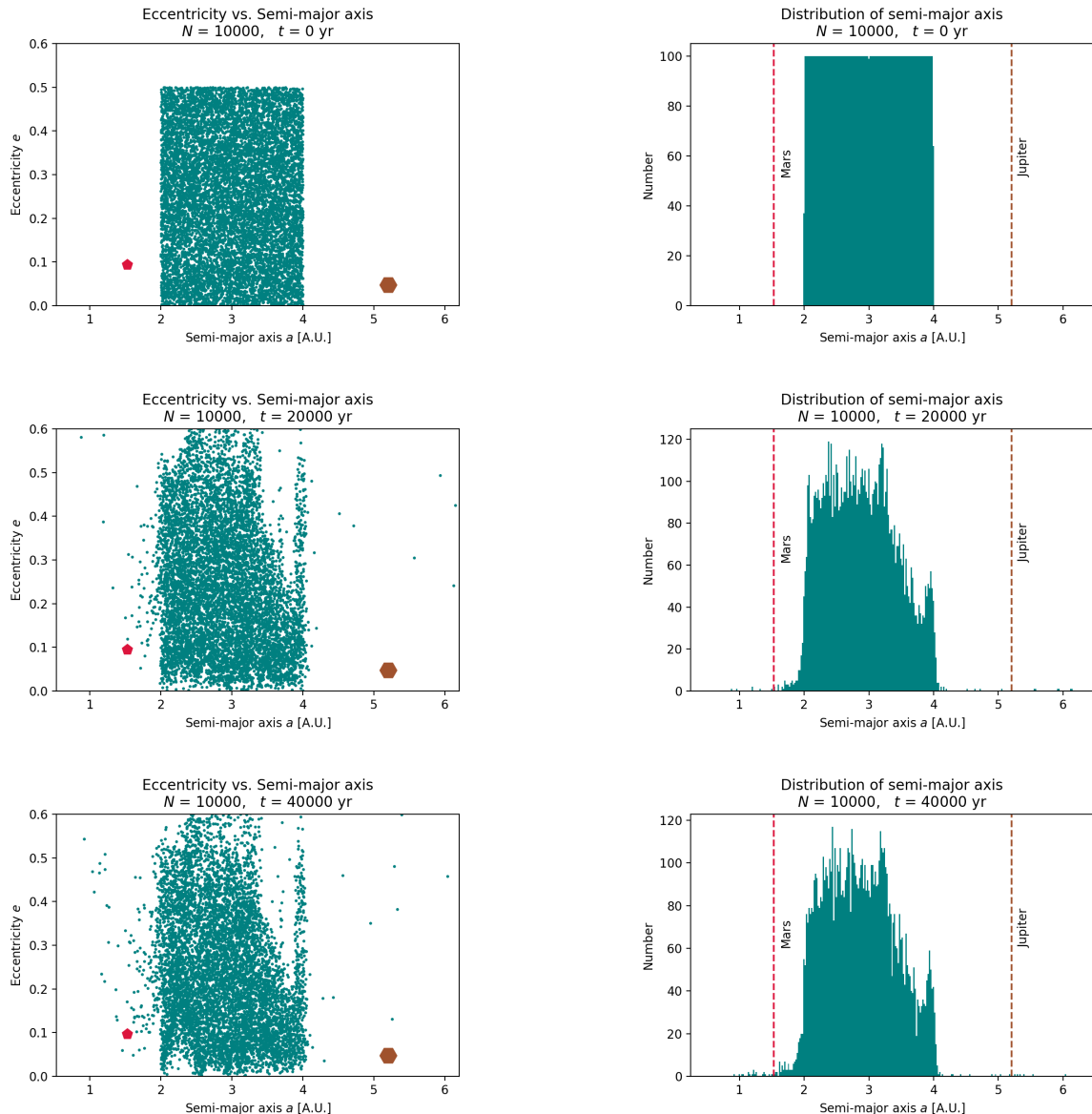


Figure 10: Eccentricity e over semi-major axis a (panels on the left column) and histogram of number of asteroids (panels on the right column); simulation time 0 years to 40 000 years.

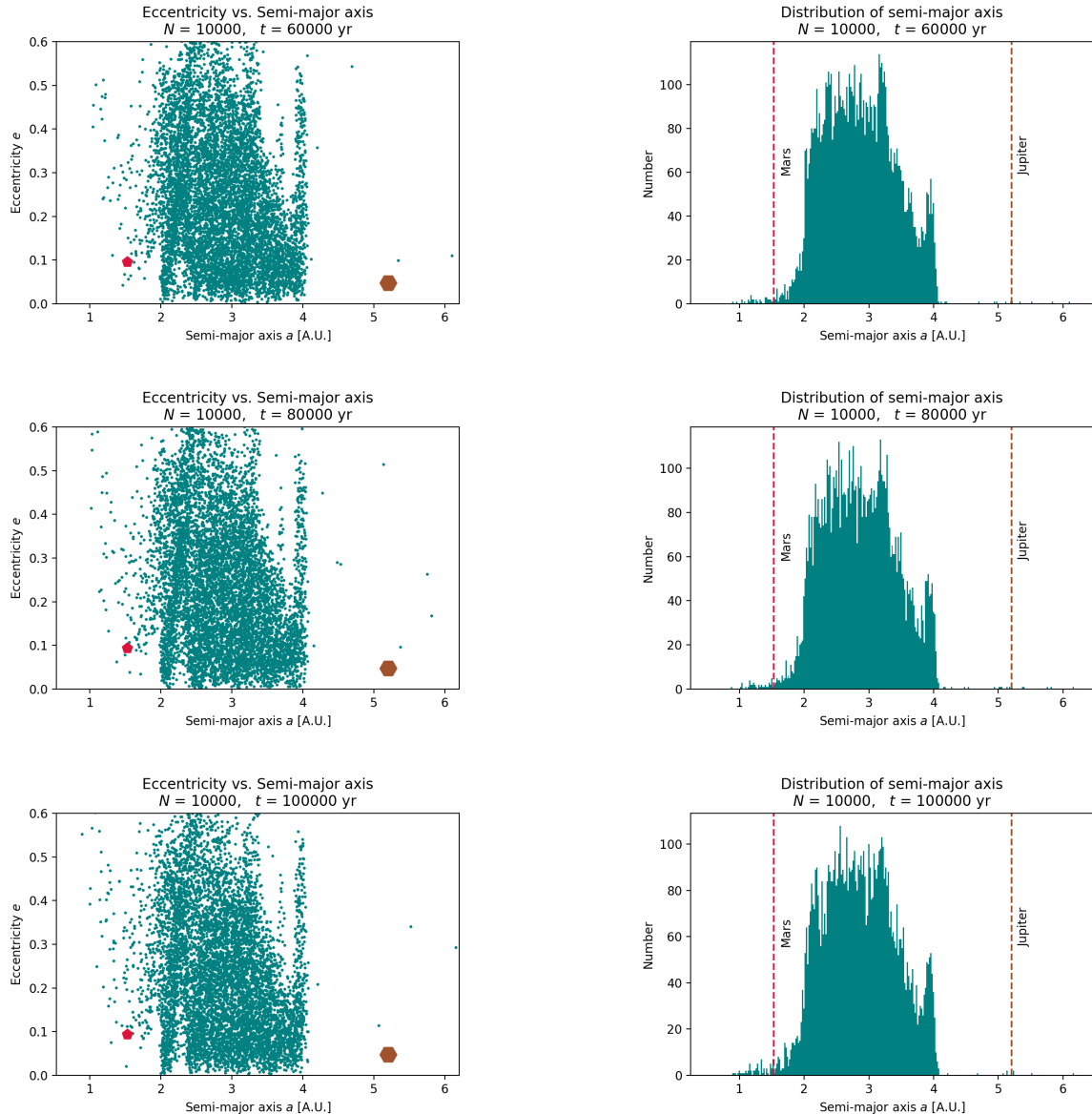


Figure 11: Eccentricity e over semi-major axis a (panels on the left column) and histogram of number of asteroids (panels on the right column); simulation time 60 000 years to 100 000 years.

In Fig. 12 we don't observe significant gaps on the distribution of semi-major axes. However, some obvious belt structure exists at 4 AU and 3.7 AU. Chances are that our labels of orbital resonances are wrong and need to be re-scaled.

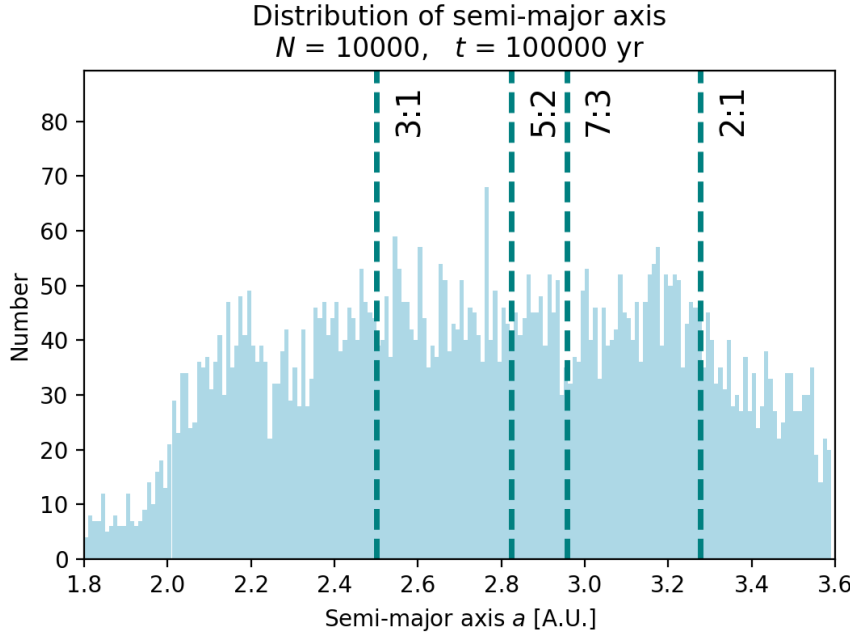


Figure 12: Histogram of number of asteroids, zoomed in between 1.8 AU to 3.6 AU. Several semi-major axes of orbital resonances with Jupiter are marked by vertical lines.

5 Resonant capture of planet

In this exercise, we study the resonant capture of a three-body system composed of a primary object and two planets. The system is initially set up using the parameters in Table 6.

We let Planet 1 migrate from 24 AU to 10 AU with an *e*-folding time of 10^5 years.³ The simulation of migration is carried out with the aid of the `exponential_migration` module in the extra library called REBOUNDx.

Table 6: Setup 1 of Section 5.

Object	m	a_i	e_i
Primary	$1 M_\odot$		
Planet 1	$5.1 \times 10^{-5} M_\odot$	24.000	0.010
Planet 2	$6.0 \times 10^{-6} M_\odot$	10.000	0.000

After the simulation is done, we will plot the evolution of some orbital parameters such as semi-major axis a , eccentricity e , and period P (Figs. 13a and 14a). To present the orbit resonance better, we will make additional plots, including the evolution of the ratio a_1/a_2 and the ratio P_1/P_2 (Figs. 13b and 14b), also the configurations of planets before and after the simulation (Figs. 13c and 14c).

³*e*-folding time is the time interval in which an exponentially decreasing (or increasing) quantity (in our case, the semi-major axis a) increases (or decreases) by a factor of $e = 2.71828\dots$. It is a measure of migration rate. The smaller *e*-folding is, the faster the migration is.

5.1 Trial 1

In the first trial, the e -folding time is 1.0×10^3 yr and the execute the simulation is 1.0×10^5 yr. The results are shown in Table 7 and Fig. 13.

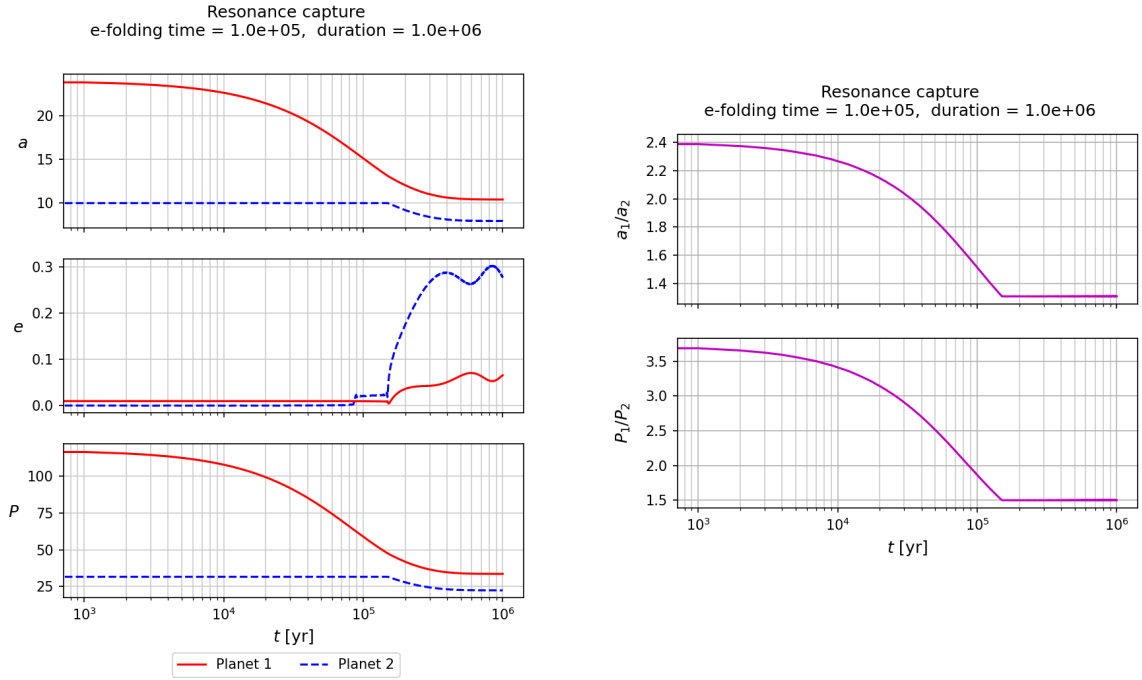
In Fig. 13b, one can observe a steady decrease on the ratio P_1/P_2 between $t = 10^4$ yr and $t = 10^5$ yr. Fig. 13b suggests that such decrease is mainly caused by the inward migration of Planet 1, while the orbit of Plant 2 is not yet affected. However, at a critical point of $t \approx 1.3 \times 10^5$ yr, eccentricities e_1 and e_2 start showing substantial changes; conversely, P_1/P_2 stops varying abruptly and remains at a constant value of 1.5, as predicted in [4]. In other words, we see Planet 2 captured by Planet 1 and conclude that both planets attain a relatively stable 3 : 2 resonance. We also note that the evolution patterns of semi-major axis and period resemble to each other, which is simply a direct consequence of Kepler's third law.

Table 7: Orbital parameters of Trial 1. Also refer to Fig. 13c.

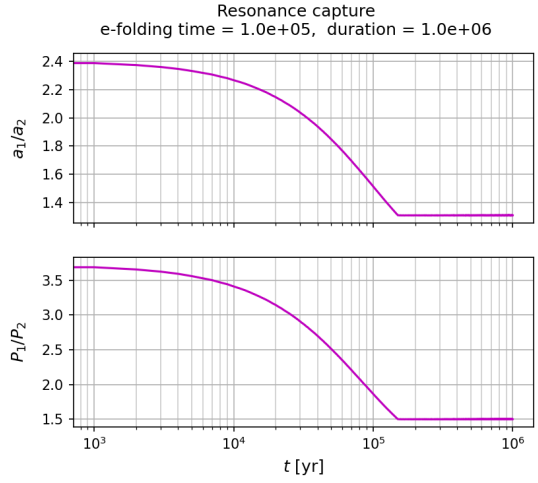
	a_i	e_i	P_i	a_f	e_f	P_f
Planet 1	24.000	0.010	117.575	10.416	0.066	33.614
Planet 2	10.000	0.000	31.622	7.948	0.278	22.407
Planet 1 : Planet 2	2.400	NaN	3.718	1.310	0.237	1.500

5.2 Trial 2

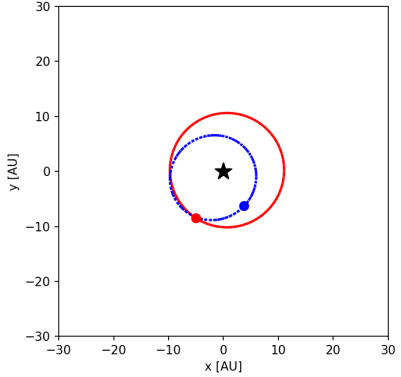
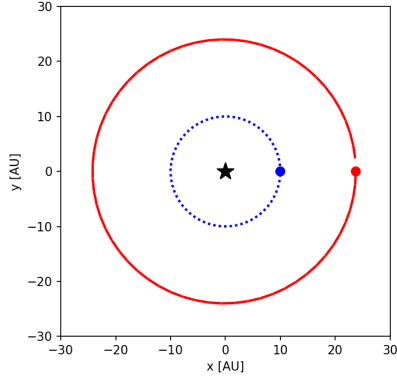
The stability of resonant capture is not always assured. To show this, we try a different e -folding time 1.0×10^3 yr and execute the simulation for 1.0×10^5 yr. The results are shown in Fig. 14. It can be seen that the early evolution patterns are similar to those in Figs. 13a and 13b, but the follow-up development, especially the eccentricity of Planet 2, is much more unstable than the former case.



(a) Evolution of semi-major axis a (top), eccentricity e (middle) and period P (bottom).



(b) Evolution of ratio of semi-major axes a_1/a_2 (upper panel) and evolution of ratio of periods P_1/P_2 (lower panel).



(c) Initial (left) and final (right) configurations. The red solid line is the trajectory of Planet 1; and blue dashed line is the trajectory of Planet 2.

Figure 13: Resonance capture with e -folding time 1.0×10^5 years and simulation duration 1.0×10^6 years.

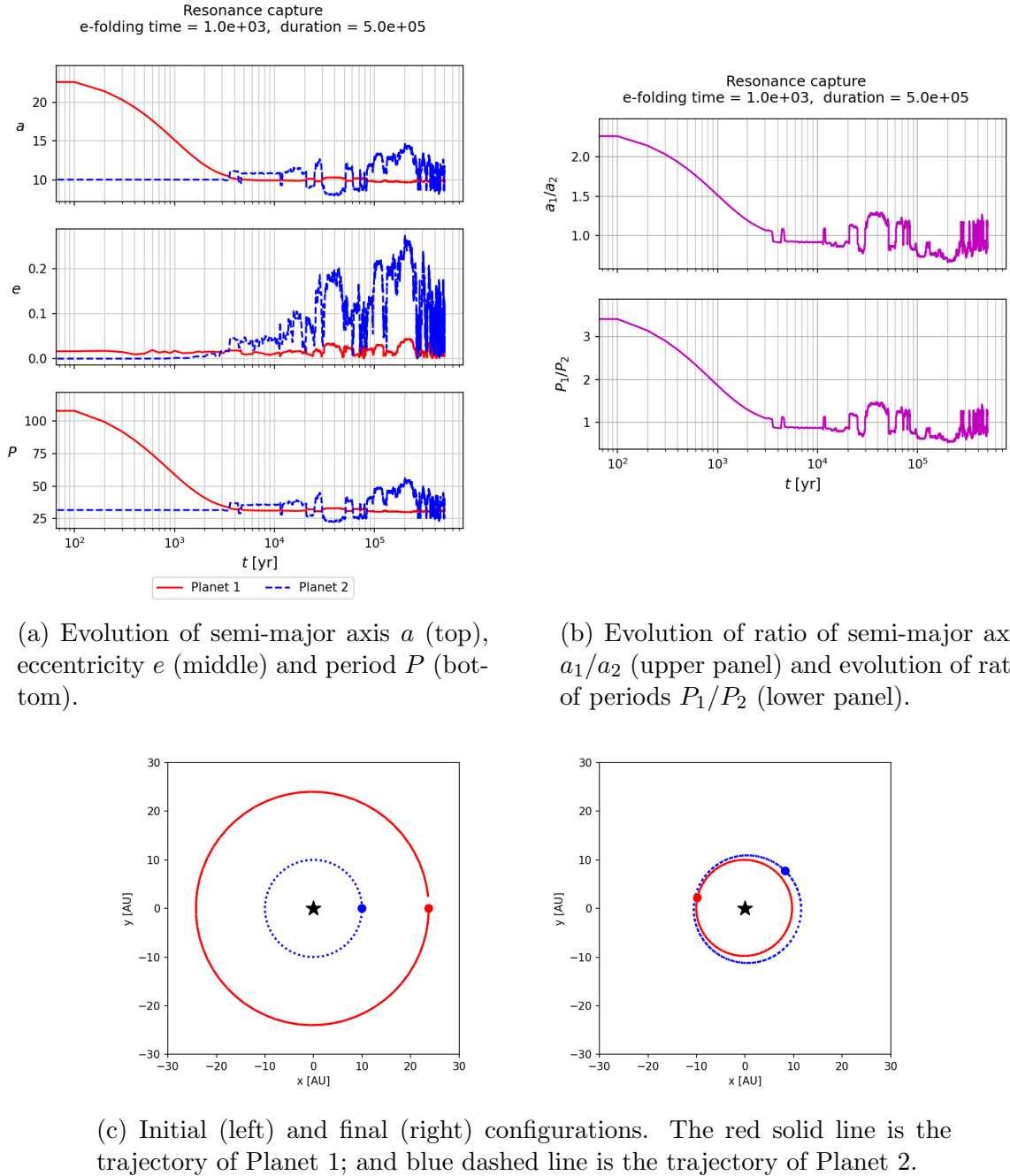


Figure 14: Resonance capture with e -folding time 1.0×10^3 years and simulation duration 5.0×10^5 years.

References

- [1] Brett Gladman. “Dynamics of Systems of Two Close Planets”. In: *Icarus* 106.1 (1993), pp. 247–263. ISSN: 0019-1035. DOI: <https://doi.org/10.1006/icar.1993.1169>.
- [2] Robert J. Vanderbei and Egemen Kolemen. “Linear Stability of Ring Systems”. In: *The Astronomical Journal* 133.2 (Jan. 2007), p. 656. DOI: [10.1086/510457](https://doi.org/10.1086/510457).
- [3] L. Niederman et al. “On the Co-orbital Motion in the Three-Body Problem: Existence of Quasi-periodic Horseshoe-Shaped Orbits.” In: *Communications in Mathematical Physics* 377 (July 2020), pp. 551–612. DOI: [10.1007/s00220-020-03690-8](https://doi.org/10.1007/s00220-020-03690-8).
- [4] Christoph Schäfer. *N-Body Simulations with REBOUND*. https://www.tat.physik.uni-tuebingen.de/~schaefer/teach/f/rebound_applications.pdf. Instruction manual of Practical Course in Astronomy at Universität Tübingen. 2022.